Please cite this article in press as: Fan et al., MiR-34a Promotes Osteogenic Differentiation of Human Adipose-Derived Stem Cells via the *RBP2/NOTCH1/CYCLIN D1* Coregulatory Network, Stem Cell Reports (2016), http://dx.doi.org/10.1016/j.stemcr.2016.06.010

Stem Cell Reports
Article

ISSCR

OPEN ACCESS

MiR-34a Promotes Osteogenic Differentiation of Human Adipose-Derived Stem Cells via the *RBP2/NOTCH1/CYCLIN D1* Coregulatory Network

Cong Fan,[1,4,5] Lingfei Jia,[2,3,4,5] Yunfei Zheng,[2,4] Chanyuan Jin,[1,4] Yunsong Liu,[1,4] Hao Liu,[3,4] and Yongsheng Zhou[1,4,*]

[1]Department of Prosthodontics
[2]Department of Oral and Maxillofacial Surgery
[3]Central Laboratory
[4]National Engineering Lab for Digital and Material Technology of Stomatology, Beijing Key Laboratory of Digital Stomatology
Peking University School and Hospital of Stomatology, Beijing 100081, China
[5]Co-first author
*Correspondence: kqzhouysh@hsc.pku.edu.cn
http://dx.doi.org/10.1016/j.stemcr.2016.06.010

SUMMARY

MiR-34a was demonstrated to be upregulated during the osteogenic differentiation of human adipose-derived stem cells (hASCs). Overexpression of miR-34a significantly increased alkaline phosphatase activity, mineralization capacity, and the expression of osteogenesis-associated genes in hASCs in vitro. Enhanced heterotopic bone formation in vivo was also observed upon overexpression of miR-34a in hASCs. Mechanistic investigations revealed that miR-34a inhibited the expression of retinoblastoma binding protein 2 (*RBP2*) and reduced the luciferase activity of reporter gene construct comprising putative miR-34a binding sites in the 3′ UTR of *RBP2*. Moreover, miR-34a downregulated the expression of *NOTCH1* and *CYCLIN D1* and upregulated the expression of *RUNX2* by targeting *RBP2*, *NOTCH1*, and *CYCLIN D1*. Taken together, our results suggested that miR-34a promotes the osteogenic differentiation of hASCs via the *RBP2/NOTCH1/CYCLIN D1* coregulatory network, indicating that miR-34a-targeted therapy could be a valuable approach to promote bone regeneration.

INTRODUCTION

Tissue engineering technology has become one of the most promising therapeutic approaches for bone regeneration in bone defects (Zou et al., 2011; Ye et al., 2011; Xiao et al., 2011). As a source of mesenchymal stem cells (MSCs), human adipose-derived stem cells (hASCs) are receiving more attention in bone tissue engineering (Bosnakovski et al., 2005; Zuk et al., 2002; Wang et al., 2011). However, the paucity of available information about the molecular pathways that govern the osteogenic differentiation of hASCs has hampered further development of hASC-based cell therapies.

MicroRNAs (miRNAs) are a class of endogenously expressed, small non-coding RNA molecules that negatively regulate gene expression at the post-transcriptional level by base pairing with the 3′ UTR of their target mRNAs (Thomas et al., 2010). They play vital roles in various biological processes, including the cell fate of embryonic stem cells, cell proliferation, apoptosis, differentiation, morphogenesis, carcinogenesis, and angiogenesis (Ambros, 2004; Hua et al., 2006; Xu et al., 2004). A single miRNA is often involved in several gene regulatory networks (Bartel, 2004; Krek et al., 2005), and overexpression or inhibition of miRNAs can regulate the endogenous expression of multiple growth factors simultaneously (Yau et al., 2012). Therefore, we hypothesized that the delivery of a desired miRNA may result in optimization of bone regeneration. Recent studies have reported that several miRNAs, such as miR-22, -100, -106a, -146a, and -148b, are involved in the osteogenic differentiation of stem cells (Cho et al., 2010; Huang et al., 2012; Li et al., 2013a; Liao et al., 2014; Qureshi et al., 2013; Zeng et al., 2012). However, further regulatory mechanisms of miRNAs in the osteogenesis of MSCs still await investigation.

Our previous study showed that the inhibition of retinoblastoma binding protein 2 (*RBP2*) significantly improved the in vitro and in vivo osteogenic capacity of hASCs (Ge et al., 2011). Based on these data, we aimed to screen and select miRNAs that positively regulate the osteogenic differentiation of hASCs by targeting *RBP2*. Microarray analyses revealed that after osteogenic induction, 21 miRNAs were upregulated in hASCs (Zhang et al., 2012) and 51 miRNAs were upregulated in bone marrow-derived MSCs (BMSCs) (Gao et al., 2011), suggesting that 72 upregulated miRNAs had potential effects on the osteogenic differentiation of MSCs. Moreover, RNA22 prediction software indicated that 122 miRNAs might bind to the 3′ UTR of *RBP2* mRNA. These two categories of miRNAs were combined and an intersection of five miRNAs was produced: miR-663, -34a, -26a, -17, and -155. The RNA22 prediction software predicted their corresponding folding energy (ΔG) was −14.00 kcal/mol, −16.8 kcal/mol, −12.50 kcal/mol, −13.20 kcal/mol, and −13.30 kcal/mol. According to the results predicted

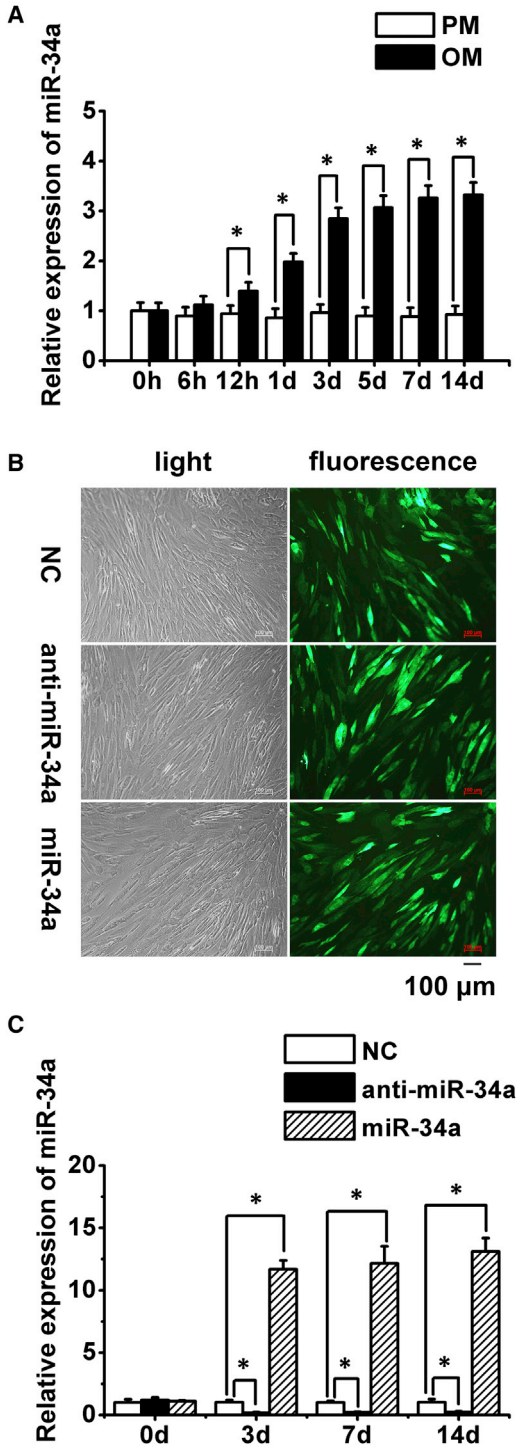

Figure 1. Expression of Endogenous miR-34a during hASCs' Osteogenic Induction, and Determination of Lentiviral Transduction Efficiency and Effect

(A) Quantitative real-time PCR analysis of miR-34a expression in hASCs cultured in PM and OM.

(B) Microscopic images of GFP-positive hASCs under ordinary and fluorescent light. Scale bar, 100 μm.

(C) Quantitative real-time PCR analysis of miR-34a in transduced hASCs cultured in PM.

PM, proliferation medium; OM, osteogenic medium; NC, lentivirus negative control; anti-miR-34a, lentivirus anti-sense miR-34a; miR-34a, lentivirus miR-34a mimics. Data represent the means ± SD of three independent experiments. *$p < 0.05$ versus the NC group.

by RNA22 prediction software, miR-34a possessed the maximum likelihood for binding to the 3′ UTR of *RBP2* mRNA ($\Delta G = -16.8$ kcal/mol); therefore, we selected miR-34a for further investigation (Figure S1).

NOTCH1 and *CYCLIN D1* are direct target genes of miR-34a in tumor cells (Hermeking, 2010; Pang et al., 2010), and have effects on the proliferation and osteogenic differentiation of MSCs by regulating runt-related transcription factor 2 (*RUNX2*) (Engin et al., 2008), a key osteogenesis-associated transcription factor. Thus, *NOTCH1* and *CYCLIN D1* pathways were integrated into our hypothetical regulatory network of miR-34a.

In this study, we investigated the functional roles of miR-34a in the osteogenic differentiation of hASCs both in vitro and in vivo, and explored whether miR-34a regulated this biological process through the *RBP2/NOTCH1/CYCLIN D1* coregulatory network. Our study provided a better understanding of the role and mechanism of miR-34a in hASCs' osteogenic differentiation and suggested that miR-34a could be a therapeutic target in future bone regeneration therapy, which will lead to advances in clinical bone tissue engineering.

RESULTS

Expression Levels of miR-34a during the Osteogenic Differentiation of hASCs

After culturing hASCs in osteogenic medium (OM) for 12 hr, miR-34a expression increased significantly, and further increased with prolonged osteogenic induction. However, no significant change was detected in hASCs cultured in proliferation medium (PM) when compared with the 0-hr time point (Figure 1A). These data suggested that miR-34a might play a role in the regulation of hASCs' osteogenic differentiation.

Promotion Effects of miR-34a on the Osteogenic Differentiation of hASCs In Vitro

The transduction efficiency of lentivirus was estimated to be 80%–90%, as evaluated by the percentage of GFP-positive cells under an inverted fluorescence microscope 72 hr after transduction (Figure 1B). Quantitative real-time PCR analysis of miR-34a expression in transduced hASCs cultured in PM at 0, 3, 7, and 14 days showed

a >10-fold increase in the miR-34a overexpression group and >75% reduction in the miR-34a knockdown group when compared with the negative control (NC) group (Figure 1C). Alkaline phosphatase staining and quantification showed that overexpression of miR-34a enhanced the osteogenic differentiation of hASCs cultured in PM or OM at 7 days, while miR-34a knockdown inhibited alkaline phosphatase activity of hASCs (Figures 2A and 2B). The extracellular mineralization of hASCs, as tested by Alizarin red S (ARS) and von Kossa staining in PM or OM at 14 days, displayed similar results to the alkaline phosphatase tests (Figures 2C–2E). Moreover, overexpression of miR-34a significantly increased the expression of osteogenesis-associated genes, including *RUNX2*, osterix (*OSX*), alkaline phosphatase (*ALP*), and osteocalcin (*OC*), while miR-34a knockdown led to the opposite tendency (Figures 2F and S2).

Promotion Effects of miR-34a on the Osteogenic Differentiation of hASCs In Vivo

Given the existence of other biological factors and the uncontrollability of the microenvironment, sometimes the in vivo results may be different and even opposite to those in vitro. Therefore, the investigation of miR-34a's in vivo effect was necessary. The microstructure of the newly formed bone was evaluated by micro-computed tomography (CT) imaging. The representative images in the blank and miR-34a knockdown groups showed less newly formed bone and more scaffold remnants. In contrast, the miR-34a overexpression group exhibited the most newly formed bone with the fewest scaffold remnants when compared with other groups (Figure 3A). By quantifying the amount of new bone, the percentages of new bone volume to tissue volume (BV/TV) in the miR-34a overexpression group showed a greater than 2-fold increase, whereas the blank and miR-34a knockdown groups showed a decrease when compared with the NC group (Figure 3B). Similarly, the bone mineral density (BMD) of the miR-34a overexpression group was the highest among these four groups, while the blank and miR-34a knockdown groups were lower than the NC group (Figure 3C).

Collagen deposition, as assessed by Masson trichrome staining, demonstrated that the most bone matrix was found in the miR-34a overexpression group (Figure 3Da). H&E staining of each group showed that no new bone was found in the blank, NC, or miR-34a knockdown group, but osteoid was formed in the miR-34a overexpression group (Figures 3Db and S3). Immunohistochemical (IHC) staining for OC indicated that both the range and intensity of the stained granules in osteoblasts were generally increased in the miR-34a overexpression group (Figure 3Dc), suggesting that miR-34a induced the expression of OC.

Direct Targeting of *RBP2* by miR-34a

RNA22 prediction software identified *RBP2* as a potential target gene of miR-34a, and *RBP2* inhibition improves the osteogenic capacity of hASCs (Ge et al., 2011); therefore, we investigated its effect on *RBP2* expression to clarify the molecular mechanism underlying the osteogenic regulation of hASCs by miR-34a. As predicted, overexpression of miR-34a resulted in downregulation of *RBP2*, whereas miR-34a knockdown increased the expression of *RBP2* at both the mRNA and protein levels (Figures 4A–4C). The putative binding sites of miR-34a in the 3′ UTR of *RBP2* was predicted by RNA22 prediction software (Figure 4D). Thus, we constructed a luciferase reporter vector (Figure 4E) to determine whether miR-34a could directly target these sites. Luciferase activity analysis showed that miR-34a repressed the luciferase expression of vectors containing the 3′ UTR of wild-type *RBP2* (*RBP2*-WT), but had no effect on the mutant-type *RBP2* (*RBP2*-MT) group compared with the NC group (Figure 4F). These results indicated that miR-34a negatively regulated *RBP2* by directly binding to the 3′ UTR of its mRNA.

Direct Repression of *NOTCH1* and *CYCLIN D1* by miR-34a

NOTCH1 and *CYCLIN D1* were previously identified as direct target genes of miR-34a in tumor cells (Hermeking, 2010; Pang et al., 2010). Moreover, the miR-34a potential target sites in *NOTCH1* and *CYCLIN D1* transcripts were predicted by RNA22 software (Figure S4). Our results confirmed that in hASCs, miR-34a overexpression suppressed the expression of *NOTCH1* and *CYCLIN D1* at both the mRNA and protein levels, while miR-34a knockdown resulted in the upregulation of these two genes (Figures 5A and 5B).

Upregulated Expression of *RUNX2* by miR-34a

Previous studies reported that *RBP2* could directly downregulate *P27*, leading to the upregulation of *CYCLIN D1* expression (Liang et al., 2013; Teng et al., 2013; Zeng et al., 2010). Thus, we explored the effect of miR-34a on *P27* expression and demonstrated that miR-34a increased the expression of *P27* at both the mRNA and protein levels (Figures 5C and 5D). Importantly, miR-34a overexpression significantly upregulated the expression of *RUNX2*, a major osteogenesis-associated transcription factor, and *RUNX2* expression was downregulated in response to miR-34a knockdown (Figures 5C and 5D).

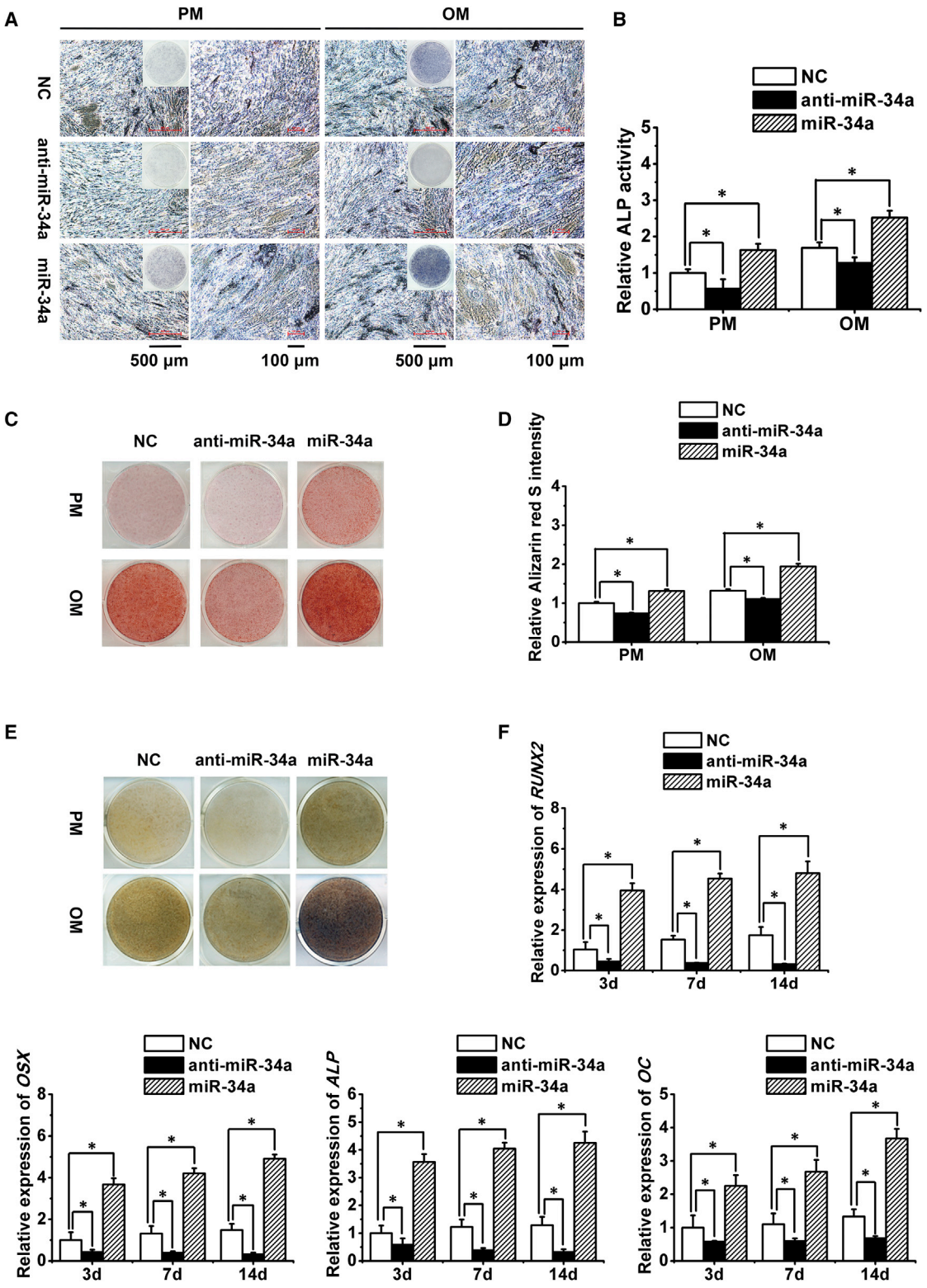

Figure 2. Promotion of hASCs' Osteogenic Differentiation by miR-34a In Vitro

(A and B) ALP staining (A) and quantification (B) of transduced hASCs. Scale bar of the left panel in PM or OM group, 500 μm; scale bar of the right panel in PM or OM group, 100 μm.

(legend continued on next page)

Coregulation of the *RBP2/NOTCH1/CYCLIN D1* Network by miR-34a in the Osteogenic Differentiation of hASCs

To further confirm the interactions among *RBP2*, *NOTCH1*, *CYCLIN D1*, and *RUNX2*, we transfected hASCs with anti-*RBP2* and anti-*NOTCH1* lentivirus and then evaluated the expression of possible downstream target genes through quantitative real-time PCR and western blotting. The transduction effects of anti-*RBP2* and anti-*NOTCH1* lentivirus showed ~50% reductions in the expression of respective genes (Figures 6A–6D). We found that *RBP2* knockdown upregulated the expression of *P27* and *RUNX2*, and downregulated *CYCLIN D1* expression (Figures 6A and 6B). Similarly, *NOTCH1* knockdown resulted in the downregulation of *CYCLIN D1* and upregulation of *RUNX2* (Figures 6C and 6D). Taken together, these results indicated that miR-34a indirectly increased the expression of *P27* and *RUNX2* by directly suppressing *RBP2*, *NOTCH1*, and *CYCLIN D1*, suggesting that miR-34a modulated the osteogenic differentiation of hASCs through the *RBP2/NOTCH1/CYCLIN D1* coregulatory network.

DISCUSSION

The development of miRNA-based therapy approaches has become one of the most attractive areas of tissue engineering (Lian et al., 2012). Recently, many studies reported that miRNAs are important regulators for the therapy or differentiation of stem cells (Cho et al., 2010; Huang et al., 2012; Li et al., 2013a; 2013b; Liao et al., 2014; Qureshi et al., 2013; Zeng et al., 2012; Deng et al., 2013). In this study, we observed a significant increase in miR-34a expression during the osteogenic differentiation of hASCs, which was consistent with previous studies (Ambros, 2004; Hua et al., 2006). This upregulation during osteogenic induction indicated that miR-34a might have an effect on the osteogenic differentiation of hASCs.

A combination of in vitro and in vivo experiments indicated that miR-34a overexpression promoted the osteogenic differentiation and ectopic osteogenesis of hASCs, while miR-34a knockdown inhibited osteogenic capacity when compared with the NC group. We found that miR-34a promoted the alkaline phosphatase activity and mineralization capacity and also increased the expression of osteogenesis-associated genes including *RUNX2*, *OSX*, *ALP*, and *OC* in both PM and OM. This indicated that miR-34a overexpression promoted osteogenic differentiation in vitro. Moreover, heterotopic bone formation after in vivo implantation of hASCs and scaffold hybrids was evaluated by micro-CT and histological staining. As stated above, the osteogenic effect of miR-34a shown in scanning images and quantitative analysis by BV/TV and BMD were in accordance with those in vitro, and histological assessment including Masson, H&E, and IHC staining verified this conclusion as well.

Although miR-34a was once reported to inhibit proliferation and osteogenic differentiation in BMSCs by targeting a number of known cell-cycle proteins and *JAGGED1* (Chen et al., 2014), two other studies report that it enhances osteogenesis by inhibiting osteoclastogenesis of osteoclasts from bone marrow (Krzeszinski et al., 2014) or promoting osteogenic differentiation of apical papilla stem cells (Sun et al., 2014). In our study, both the mRNA and protein expression of *JAGGED1* did not show significant difference by overexpressing or knocking down miR-34a in hASCs (Figure S5). The contradictory results might partly be attributed to the varied characteristics of the different cell lines and distinct post-transcriptional regulation of the osteogenic differentiation in tissue-specific MSCs. In addition, Park et al. (2015) found that overexpression of miR-34a decreased the cell proliferation and downregulated the expression of various cell-cycle regulators such as *CDK*s (*-2*, *-4*, *-6*) and *CYCLIN*s (*-E*, *-D*). These results were consistent with ours, but found too that the potential of adipogenesis and osteogenesis of hASCs was also diminished by miR-34a overexpression. As we know, a mutually exclusive relationship usually exists between osteoblastogenesis and adipogenesis, with factors stimulating one of these processes while at the same time inhibiting the other (Huang et al., 2012; Wang et al., 2013). Thus we need to further investigate the effects of miR-34a on the osteogenesis and adipogenesis of hASCs. Moreover, there are some reports concerning the contradictory effects of other miRNAs on osteogenic differentiation. For example, miR-26a can either promote (Wang et al., 2015a; 2015b) or suppress (Luzi et al., 2008, 2012) the osteogenic differentiation of hASCs. Therefore, further research is needed to elucidate the osteogenic regulation of miRNAs. Taken together, our study

(C and D) ARS staining (C) and quantification (D) of transduced hASCs.

(E) von Kossa staining of transduced hASCs.

(F) Quantitative real-time PCR analysis of *RUNX2*, *OSX*, *ALP*, and *OC* expression in transduced hASCs.

ALP, alkaline phosphatase; ARS, Alizarin red S; *RUNX2*, runt-related transcription factor 2; *OSX*, osterix; *OC*, osteocalcin. Data represent the means ± SD of three independent experiments. *$p < 0.05$ versus the NC group.

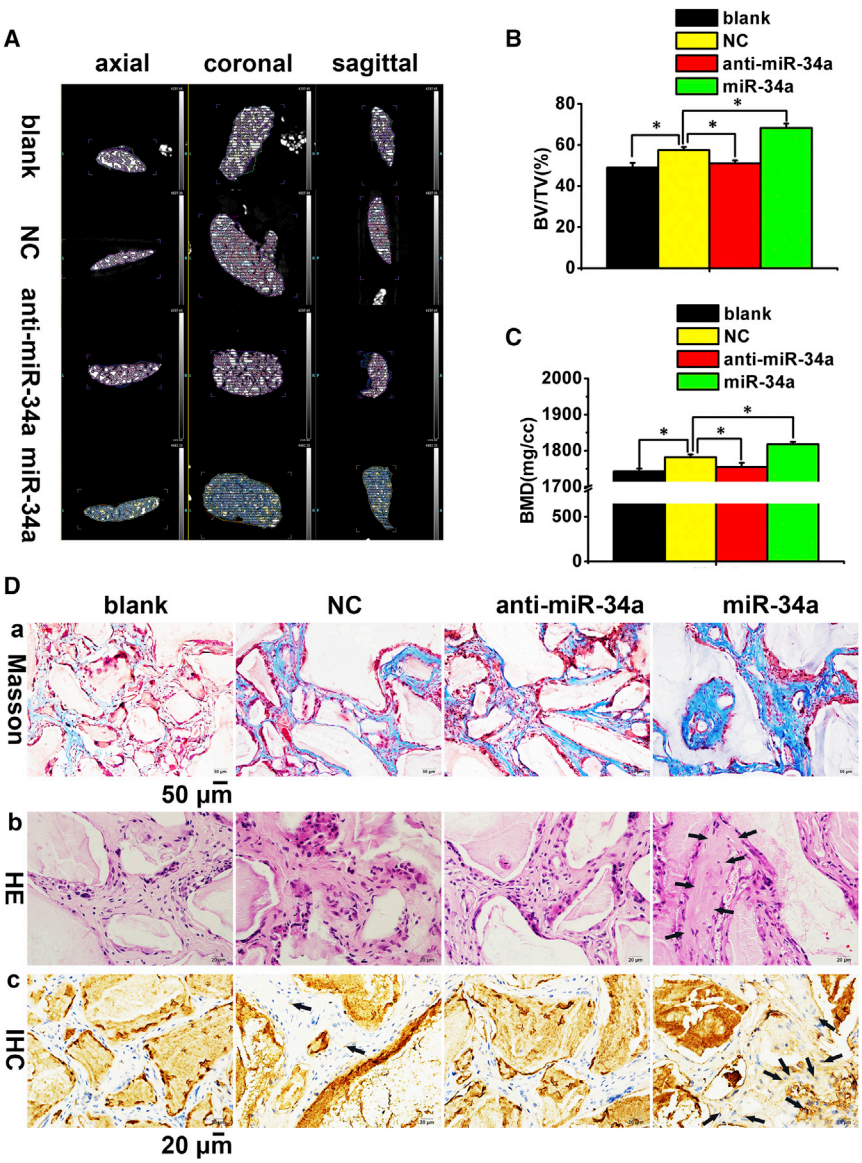

Figure 3. Promotion of hASCs' Osteogenic Differentiation by miR-34a In Vivo

(A) Newly formed bone in Bio-Oss collagen scaffolds are indicated in different colors; scaffold remnants appear as white irregular lumps.

(B and C) Quantitative analysis of BV/TV and BMD. Data represent the means ± SD of three independent experiments. *$p < 0.05$ versus the NC group.

(D) Histological assessment of ectopic bone formation. (a) Masson trichrome staining. The collagen in the bone matrix was stained blue-green. (b) H&E staining. New bone structures are indicated by black arrows. (c) IHC staining for OC. Dark-brown granules indicating positive staining are marked by black arrows. Scale bar, 50 μm in (a) and 20 μm in (b) and (c).

BV/TV, percentage of new bone volume to tissue volume; BMD, bone mineral density; IHC, immunohistochemistry; blank, scaffolds without hASCs; NC/anti-miR-34a/miR-34a, scaffolds seeded with hASCs transfected by lentivirus negative control/anti-sense miR-34a/miR-34a mimics.

indicated that other signal molecules and pathways might be involved in the regulation of osteogenic differentiation by miR-34a.

Furthermore, we demonstrated that *RBP2* was a target gene of miR-34a in hASCs. MiR-34a repressed the luciferase activity of reporter vectors containing putative binding sites in the 3′ UTR of *RBP2*, indicating that miR-34a directly binds to the 3′ UTR of *RBP2* mRNA. In addition, *RBP2* directly binds to the promoter of *P27* (Liang et al., 2013; Teng et al., 2013; Zeng et al., 2010), which is a member of cyclin-dependent kinase inhibitors (*CDKIs*) and plays a critical role in inhibiting the transition of the cell cycle from the G1 to the S phase by binding and inhibiting *CYCLIN*/*CDKs*, including *CYCLIN D1* (Perisanidis et al., 2012; Pestell, 2013; Wang et al., 2012; Zhang et al., 2014b; Chen et al., 2013). In the present study, both miR-34a overexpression and *RBP2* knockdown caused upregulation of *P27* and downregulation of *CYCLIN D1*, suggesting the suppressed proliferation of hASCs. Moreover, we previously demonstrated that *RBP2* physically and genetically repressed the transcriptional activity of *RUNX2* (Ge et al., 2011). The upregulation of *RUNX2* after knockdown of *RBP2* confirmed this conclusion. These results suggested that miR-34a could upregulate the expression of *RUNX2* by directly binding to the *RBP2* mRNA.

Our study also confirmed that miR-34a overexpression induced the downregulation of *NOTCH1* and *CYCLIN D1*, which have been identified as target genes of miR-34a in tumor cells (Wei et al., 2012; Bae et al., 2012; Li

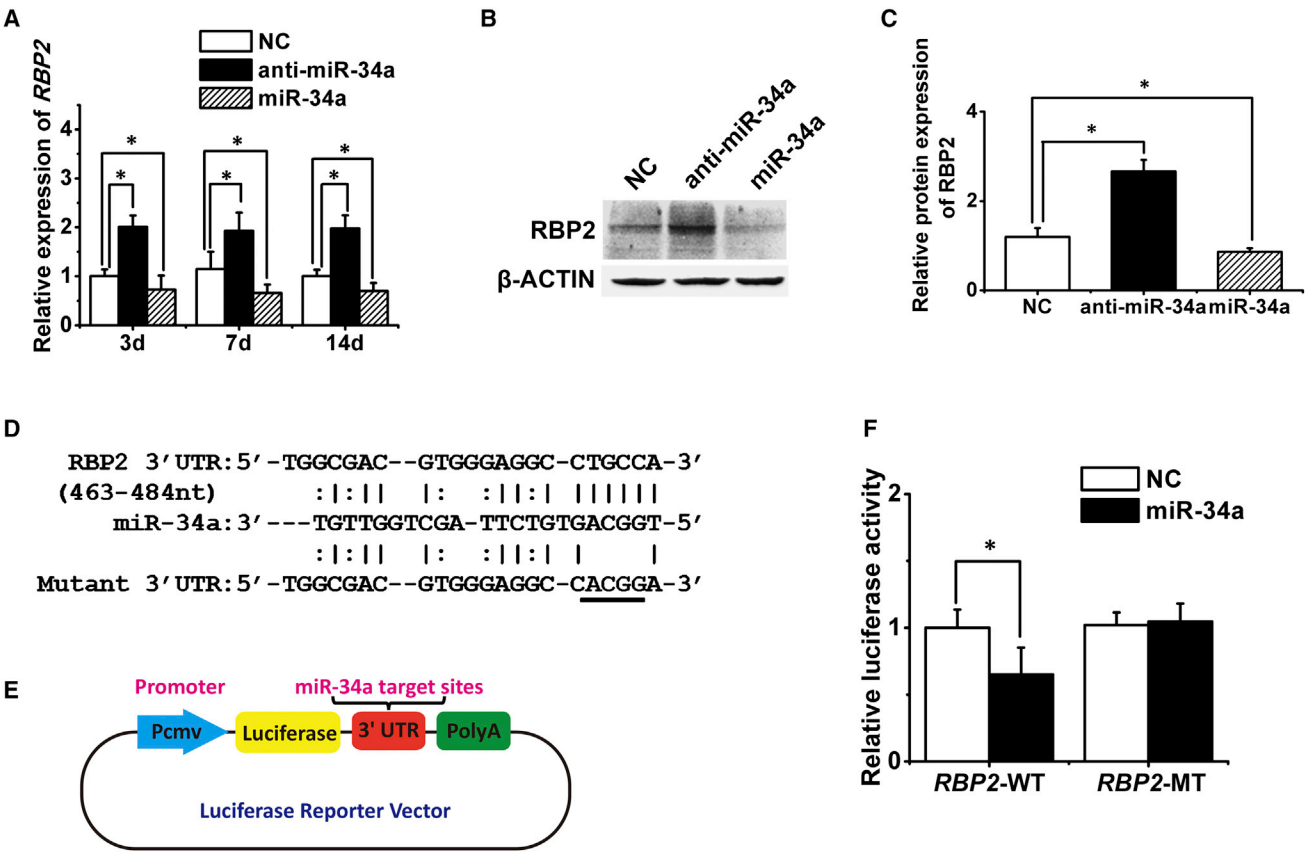

Figure 4. Validation of *RBP2* as a Direct Target Gene of miR-34a

(A–C) Quantitative real-time PCR (A) and western blotting (B and C) analysis of the effects of miR-34a on *RBP2* expression.

(D) Predicted binding sites of miR-34a in the 3′ UTR of *RBP2*-WT mRNA (underlined part indicates mutated base sequences in the 3′ UTR of *RBP2*-MT).

(E) Schematic showing the constructed luciferase reporter system containing the binding sites of miR-34a.

(F) Luciferase activity of cells with miR-34a overexpression in the *RBP2*-WT or *RBP2*-MT group.

RBP2, retinoblastoma binding protein 2; *RBP2*-WT, wild-type RBP2 mRNA; *RBP2*-MT, mutant-type RBP2 mRNA. Data represent the means ± SD of three independent experiments. *$p < 0.05$ versus the NC group.

et al., 2012; Sun et al., 2008; Zhang et al., 2014a). In addition, *CYCLIN D1* is a direct target gene of *NOTCH1* (Perisanidis et al., 2012; Cohen et al., 2010). We found that *CYCLIN D1* expression was reduced significantly after knockdown of *NOTCH1*. Moreover, gain of *NOTCH* inhibits osteoblast maturation by directly repressing *RUNX2*, as well as by repressing the anti-proliferative effects of *RUNX2* via *CYCLIN D1* upregulation (Engin et al., 2008). This study showed upregulated expression of *RUNX2* in hASCs with *NOTCH1* knockdown. Our current findings and those from previous studies suggested that miR-34a could also upregulate the expression of *RUNX2* by directly depressing *NOTCH1* and *CYCLIN D1* expression.

RUNX2 is an important osteoblast lineage-determining transcription factor that induces the expression of bone sialoprotein (*BSP*), *OC*, *OSX*, and osteopontin (*OPN*), which are required to finalize terminal osteogenic differentiation (Komori, 2002, 2003, 2008). The key effect of *RUNX2* in osteogenesis is suppressing osteoblast proliferation and promoting osteoblast maturation by supporting exit from the cell cycle (Galindo et al., 2005; Pratap et al., 2003). Our study proved that overexpression of miR-34a and knockdown of *RBP2* or *NOTCH1* eventually induced the upregulation of *RUNX2*, which probably accounted for the positive regulation of hASCs' osteogenic differentiation by miR-34a.

Our sorting data displayed the interrelationship between miR-34a, *RBP2*, *NOTCH1*, *CYCLIN D1*, and *RUNX2*. The positive effect of miR-34a on hASCs' osteogenic differentiation could be attributed to the ultimate downregulation of *CYCLIN D1* and upregulation of *RUNX2* via the *RBP2/NOTCH1/CYCLIN D1* coregulatory network, which might result in the inhibition of proliferation and promotion

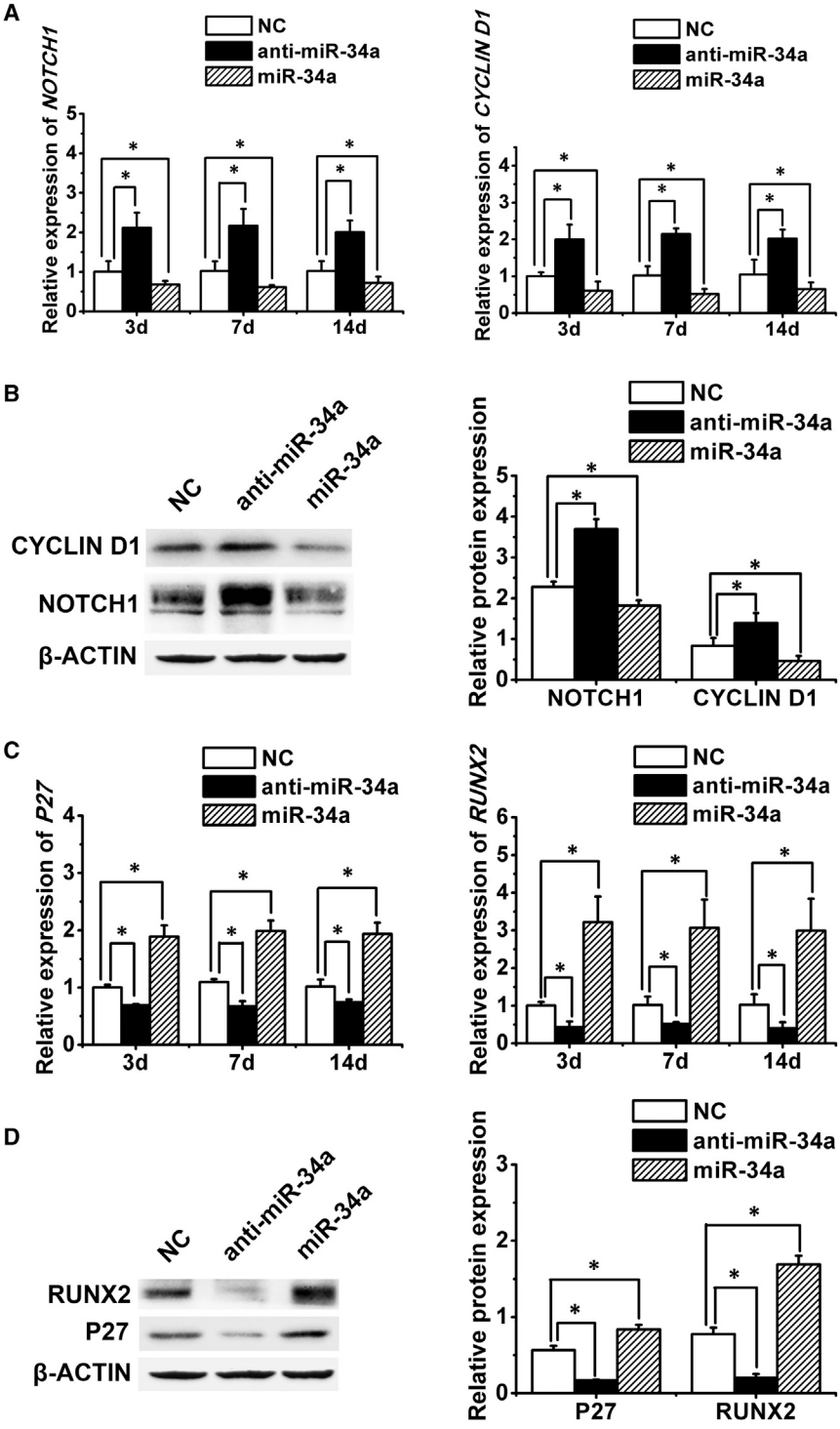

Figure 5. miR-34a Repressed *NOTCH1* and *CYCLIN D1* Expression and Upregulated *P27* and *RUNX2* Expression

(A and B) Quantitative real-time PCR (A) and western blotting (B) analysis of *NOTCH1* and *CYCLIN D1* with miR-34a knockdown or overexpression.

(C and D) Quantitative real-time PCR (C) and western blotting (D) analysis of *P27* and *RUNX2* with miR-34a knockdown or overexpression.

Data represent the means ± SD of three independent experiments. *$p < 0.05$ versus the NC group.

of osteogenic differentiation in hASCs (Figure 7). These findings supported miR-34a as a potential target for bone tissue engineering and provided valuable information on the management of bone-related diseases via epigenetic intervention.

EXPERIMENTAL PROCEDURES

Cell Culture and Osteogenic Differentiation

The hASCs and 293T cells were obtained separately from ScienCell Research Laboratories and the American Type Culture

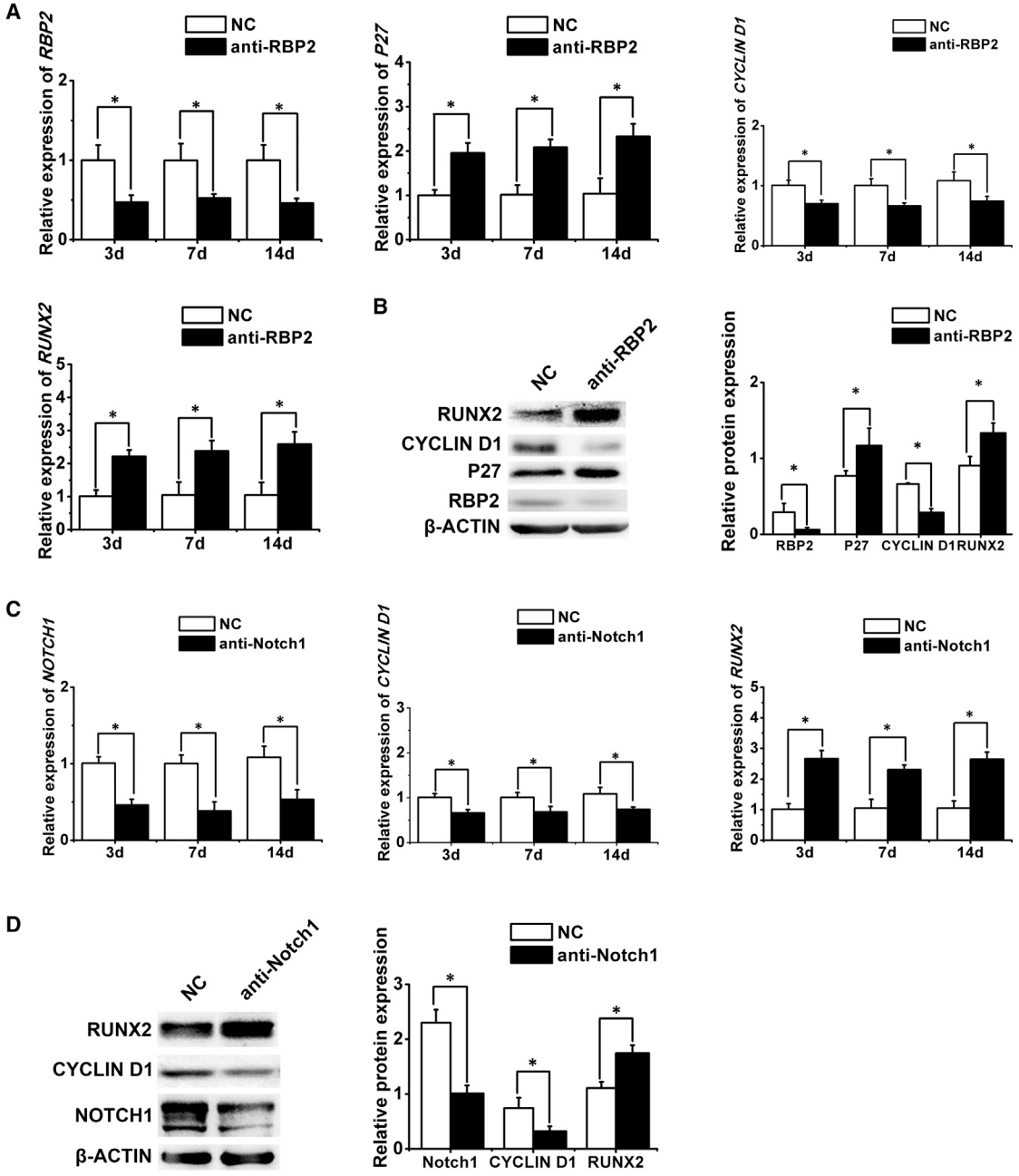

Figure 6. Confirmation of the Relationships among *RBP2*, *NOTCH1*, *P27*, *CYCLIN D1*, and *RUNX2*

(A and B) Quantitative real-time PCR (A) and western blotting (B) analysis of *RBP2*, *P27*, *CYCLIN D1*, and *RUNX2* expression after *RBP2* knockdown.

(C and D) Quantitative real-time PCR (C) and western blotting (D) analysis of *NOTCH1*, *CYCLIN D1*, and *RUNX2* expression after *NOTCH1* knockdown.

Data represent the means ± SD of three independent experiments. *$p < 0.05$ versus the NC group.

Collection. Stem cells from three donors of the third passage were used for the in vitro and in vivo experiments. All cell-based experiments were repeated three times using hASCs from the three donors, respectively. Cells were cultured in PM containing DMEM supplemented with 10% fetal bovine serum and 1% penicillin/streptomycin. Osteogenic differentiation of hASCs was induced after the cells reached 70%–80% confluence using OM (standard PM supplemented with 100 nM dexamethasone, 0.2 mM ascorbic acid, and 10 mM β-glycerophosphate).

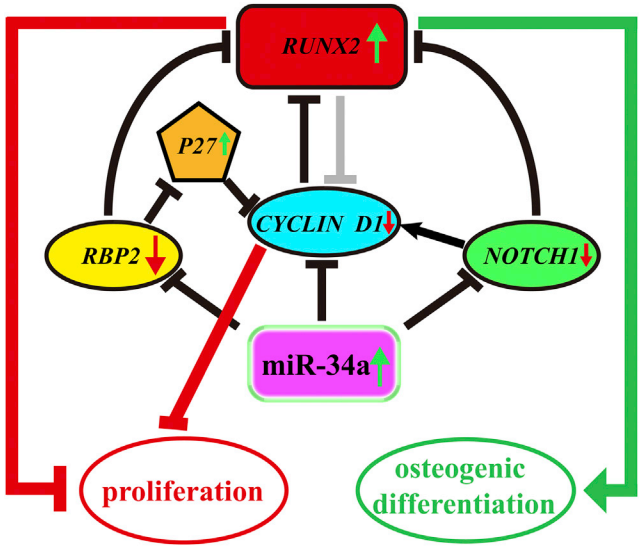

Figure 7. Schematic Representation of the *RBP2/NOTCH1/CYCLIN D1* Coregulatory Network Involved in the Osteogenic Differentiation of hASCs by miR-34a

MiR-34a directly targeted the *RBP2*, *NOTCH1*, and *CYCLIN D1* transcripts, leading to the downregulation of these target genes and subsequent upregulation of *P27* and *RUNX2*. The final repression of *CYCLIN D1* and upregulation of *RUNX2* mediated a switch from proliferation to osteogenic differentiation in hASCs.

Lentivirus Transduction and Establishment of Stably Expressing Transductants

Lentivirus containing GFP-labeled plasmid vectors of the negative control (NC), anti-sense miR-34a (anti-miR-34a), miR-34a mimics (miR-34a), *RBP2* short hairpin RNA (shRNA) (anti-*RBP2*), and *NOTCH1* shRNA (anti-*NOTCH1*) were synthesized and packaged by GenePharma. The hASCs were stably transfected with these lentiviruses at an MOI of 50 in the presence of 8 μg/ml polybrene (Sigma). After 24 hr, the lentivirus-containing medium was removed and replaced with fresh medium. Transduction efficiency was evaluated by the percentage of GFP-positive cells observed under an inverted fluorescence microscope (Nikon, TE2000-U). Puromycin at 1 μg/ml was used to select infected cells.

Alkaline Phosphatase Staining and Quantification

The hASCs were seeded at a density of 2×10^5 cells per well in 24-well plates and transfected with the lentiviruses mentioned above. Cells were cultured in PM or OM for 7 days and then evaluated for alkaline phosphatase activity. Alkaline phosphatase staining was performed using an NBT/BCIP staining kit (CoWin Biotech) with nitroblue tetrazolium (NBT) and 5-bromo-4-chloro-3-indolyl phosphate (BCIP). For quantification of alkaline phosphatase activity, cells were rinsed three times with PBS followed by 1% Triton X-100, scraped in distilled water, and subjected to three freeze-thaw cycles. The alkaline phosphatase activity was determined at 405 nm using p-nitrophenyl phosphate as the substrate. The total protein content was determined using the BCA method with the Pierce BCA protein assay kit (Thermo Scientific). Aliquots of the same samples were read at 562 nm and calculated against a series of BSA standards. Relative alkaline phosphatase activity was compared with that in the controls and calculated after normalization to the total protein content.

Mineralization Assays and Von Kossa Staining

The infected hASCs were cultured in 24-well plates with PM or OM for 14 days, and matrix mineralization was determined by ARS (Sigma) and von Kossa staining. ARS staining and quantification were performed as follows. Plates were washed three times with PBS and then stained with 0.1% ARS in distilled water (pH 4.2) for 1 hr at room temperature. After staining, the cultures were washed three times with distilled water. For quantification of matrix mineralization, ARS-stained cultures were incubated in 100 mM cetylpyridinium chloride (Sigma) for 1 hr to solubilize and release calcium-bound ARS into solution. The absorbance of the released ARS was measured at 562 nm. Relative ARS intensity was compared with that in the control treatment and calculated after normalization to the total protein content. For von Kossa staining, culture plates were fixed in 4% paraformaldehyde for 30 min and washed three times with PBS, then 1 ml of 5% silver nitrate was added and the cells were exposed to a 100 W UV lamp for 60 min. After being washed with distilled water three times, 1 ml of 5% sodium thiosulfate solution was added for 2 min and rinsed with distilled water. Finally, the mineralized extracellular matrix was observed under the microscope.

RNA Extraction, Reverse Transcription, and Quantitative Real-Time PCR

Total cellular RNA from infected hASCs cultured in PM or OM (both for 3, 7, and 14 days) were isolated using TRIzol reagent (Invitrogen) and used for first-strand cDNA synthesis with a Reverse Transcription System (Takara). Quantification of all gene transcripts was performed by quantitative real-time PCR using a Power SYBR Green PCR Master Mix (Roche) and a 7500 Real-Time PCR Detection System (Applied Biosystems). The following thermal settings were used: 95°C for 10 min, followed by 40 cycles of 95°C for 15 s and 60°C for 1 min. The internal control for mRNAs and miR-34a were *GAPDH* and *U6*, respectively (Ge et al., 2014). The products of quantitative real-time PCR were sequenced as previously described (Jia et al., 2014). The primers used are listed in Table S1. The data were analyzed using the $2^{-\Delta\Delta Ct}$ method.

Western Blotting

Western blotting was performed as described previously (Jia et al., 2014). Primary antibodies against RBP2, NOTCH1, P27, CYCLIN D1, RUNX2, and β-ACTIN (all from Cell Signaling Technology; catalog numbers 3876, 3608, 3686, 2978, 8486, and 4970, respectively) were diluted 1:1,000 and incubated with the blots at 4°C overnight. Horseradish peroxidase-conjugated anti-rabbit secondary antibodies (Cell Signaling Technology) were diluted 1:10,000 and incubated at room temperature for 1 hr.

Reporter Vectors Construction and Dual-Luciferase Reporter Assay

The functional alignment of the target region of *RBP2* was predicted by RNA22 prediction software. The 3′ UTR of *RBP2*,

containing the predicted miR-34a binding sites, were synthesized and cloned into a modified version of pcDNA3.1(+) that contained a firefly luciferase reporter gene (a gift from Brigid L.M. Hogan, Duke University), at a position downstream of the luciferase reporter gene, thus forming a wild-type (WT)-*RBP2* luciferase reporter plasmid. Site-directed mutagenesis of the miR-34a binding site in the *RBP2* 3′ UTR was performed using a Site-Directed Mutagenesis Kit (SBS Genetech) and named as mutant-type (MT)-*RBP2* luciferase reporter plasmid. All constructs were confirmed by DNA sequencing. Luciferase assays were performed as described previously (Jia et al., 2014). In brief, 293T cells at a density of 5×10^4 per well were grown in a 48-well plate and expanded to 10^5 per well before being transfected with 400 ng of either pcDNA3.0 or pcDNA3.0-miR-34a, 40 ng of the firefly luciferase reporter plasmid (*RBP2*-WT or -MT), and 4 ng of pRL-TK, a plasmid expressing Renilla luciferase (Promega). Luciferase activity was measured 24 hr after transfection using the Dual-Luciferase Reporter Assay System (Promega). Firefly luciferase activity was normalized to Renilla luciferase activity for each transfected well. Each experiment was repeated in triplicate.

In Vivo Implantation of hASCs and Bio-Oss Collagen Scaffold Hybrids

The hASCs of the third passage transfected with lentivirus (NC, anti-miR-34a, and miR-34a) were cultured in PM before the in vivo study. After being trypsinized and resuspended directly in DMEM, the cells were incubated with $6 \times 4 \times 2$ mm^3 Bio-Oss collagen scaffolds (Geistlich; GEWO) for 1 hr at 37°C, followed by centrifugation at 150 g for 5 min, and implanted into four symmetrical sites, together with blank scaffolds (without cells), on the dorsal subcutaneous space of 5-week-old, BALB/c homozygous nude (nu/nu) mice (n = 6 per group). This study was approved by the Institutional Animal Care and Use Committee of the Peking University Health Science Center (LA2014233), and all animal experiments were performed in accordance with the Institutional Animal Guidelines.

Analyses of Bone Formation In Vivo

Specimens were harvested 6 weeks after implantation, and the animals were euthanized by CO_2 asphyxiation. After fixation in 4% paraformaldehyde, the specimens were analyzed using a high-resolution Inveon micro-CT (Siemens). In brief, an X-ray voltage of 80 kV, a node current of 500 μA, and an exposure time of 500 ms for each of the 360 rotational steps were used. For quantitative analysis of the images, percentages of BV/TV and BMD were calculated (Inveon Research Workplace). The specimens were then decalcified in 10% EDTA (pH 7.4) for 14 days, followed by embedding in paraffin. Sections (5 μm thickness) were cut and stained with Masson trichrome and H&E. Meanwhile, IHC staining was also performed with primary antibodies against OC (Santa Cruz Biotechnology, catalog no. sc-240750) to evaluate osteogenesis. Finally, the tissue slices were observed under a light microscope (Olympus).

Statistical Analysis

Statistical analysis was performed using SPSS Statistics 20.0 software (IBM). Differences between two groups were analyzed by Student's t test. In cases of multiple-group testing, one-way ANOVA in conjugation with Tukey's test was conducted. A two-tailed value of $p < 0.05$ was considered statistically significant. All data are presented as the means ± SD of three independent experiments.

SUPPLEMENTAL INFORMATION

Supplemental Information includes five figures and one table and can be found with this article online at http://dx.doi.org/10.1016/j.stemcr.2016.06.010.

AUTHOR CONTRIBUTIONS

C.F., L.J., and Y.Z. designed and conducted experiments, collected and analyzed data, and wrote the manuscript. C.J., H.L., and Y.L. assisted in conducting experiments and analyzed data. Y.Z. designed the concept, and wrote and approved the manuscript.

ACKNOWLEDGMENTS

This study was financially supported by grants from the National Natural Science Foundation of China (No. 81371118), the Program for New Century Excellent Talents in University from Ministry of Education of China (NCET-11-0026), and the Ph.D. Programs Foundation of Ministry of Education of China (No. 20130001110101).

Received: December 29, 2015
Revised: June 23, 2016
Accepted: June 23, 2016
Published: July 21, 2016

REFERENCES

Ambros, V. (2004). The functions of animal microRNAs. Nature *431*, 350–355.

Bae, Y., Yang, T., Zeng, H.C., Campeau, P.M., Chen, Y., Bertin, T., Dawson, B.C., Munivez, E., Tao, J., and Lee, B.H. (2012). miRNA-34c regulates Notch signaling during bone development. Hum. Mol. Genet. *21*, 2991–3000.

Bartel, D.P. (2004). MicroRNAs: genomics, biogenesis, mechanism, and function. Cell *116*, 281–297.

Bosnakovski, D., Mizuno, M., Kim, G., Takagi, S., Okumura, M., and Fujinaga, T. (2005). Isolation and multilineage differentiation of bovine bone marrow mesenchymal stem cells. Cell Tissue Res. *319*, 243–253.

Chen, X., Zhang, T., Shi, J., Xu, P., Gu, Z., Sandham, A., Yang, L., and Ye, Q. (2013). Notch1 signaling regulates the proliferation and self-renewal of human dental follicle cells by modulating the G1/S phase transition and telomerase activity. PLoS One *8*, e69967.

Chen, L., Holmstrøm, K., Qiu, W., Ditzel, N., Shi, K., Hokland, L., and Kassem, M. (2014). MicroRNA-34a inhibits osteoblast differentiation and in vivo bone formation of human stromal stem cells. Stem Cells *32*, 902–912.

Cho, H.H., Shin, K.K., Kim, Y.J., Song, J.S., Kim, J.M., Bae, Y.C., Kim, C.D., and Jung, J.S. (2010). NF-κB activation stimulates osteogenic differentiation of mesenchymal stem cells derived from human adipose tissue by increasing TAZ expression. J. Cell Physiol. *223*, 168–177.

Cohen, B., Shimizu, M., Izrailit, J., Ng, N.F., Buchman, Y., Pan, J.G., Dering, J., and Reedijk, M. (2010). Cyclin D1 is a direct target of JAG1-mediated Notch signaling in breast cancer. Breast Cancer Res. Treat. *123*, 113–124.

Deng, Y., Zhou, H., Zou, D., Xie, Q., Bi, X., Gu, P., and Fan, X. (2013). The role of miR-31-modified adipose tissue-derived stem cells in repairing rat critical-sized calvarial defects. Biomaterials *34*, 6717–6728.

Engin, F., Yao, Z., Yang, T., Zhou, G., Bertin, T., Jiang, M.M., Chen, Y., Wang, L., Zheng, H., Sutton, R.E., et al. (2008). Dimorphic effects of Notch signaling in bone homeostasis. Nat. Med. *14*, 299–305.

Galindo, M., Pratap, J., Young, D.W., Hovhannisyan, H., Im, H.J., Choi, J.Y., Lian, J.B., Stein, J.L., Stein, G.S., and van Wijnen, A.J. (2005). The bone-specific expression of Runx2 oscillates during the cell cycle to support a G1-related antiproliferative function in osteoblasts. J. Biol. Chem. *280*, 20274–20285.

Gao, J., Yang, T., Han, J., Yan, K., Qiu, X., Zhou, Y., Fan, Q., and Ma, B. (2011). MicroRNA expression during osteogenic differentiation of human multipotent mesenchymal stromal cells from bone marrow. J. Cell Biochem. *112*, 1844–1856.

Ge, W., Shi, L., Zhou, Y., Liu, Y., Ma, G.E., Jiang, Y., Xu, Y., Zhang, X., and Feng, H. (2011). Inhibition of osteogenic differentiation of human adipose-derived stromal cells by retinoblastoma binding protein 2 repression of RUNX2-activated transcription. Stem Cells *29*, 1112–1125.

Ge, W., Liu, Y., Chen, T., Zhang, X., Lv, L., Jin, C., Jiang, Y., Shi, L., and Zhou, Y. (2014). The epigenetic promotion of osteogenic differentiation of human adipose-derived stem cells by the genetic and chemical blockade of histone demethylase LSD1. Biomaterials *35*, 6015–6025.

Hermeking, H. (2010). The miR-34 family in cancer and apoptosis. Cell Death Differ. *17*, 193–199.

Hua, Z., Lv, Q., Ye, W., Wong, C.K., Cai, G., Gu, D., Ji, Y., Zhao, C., Wang, J., Yang, B.B., et al. (2006). MiRNA-directed regulation of VEGF and other angiogenic factors under hypoxia. PLoS One *1*, e116.

Huang, S., Wang, S., Bian, C., Yang, Z., Zhou, H., Zeng, Y., Li, H., Han, Q., and Zhao, R.C. (2012). Upregulation of miR-22 promotes osteogenic differentiation and inhibits adipogenic differentiation of human adipose tissue-derived mesenchymal stem cells by repressing HDAC6 protein expression. Stem Cells Dev. *21*, 2531–2540.

Jia, L.F., Wei, S.B., Mitchelson, K., Gao, Y., Zheng, Y.F., Meng, Z., Gan, Y.H., and Yu, G.Y. (2014). MiR-34a inhibits migration and invasion of tongue squamous cell carcinoma via targeting MMP9 and MMP14. PLoS One *9*, e108435.

Komori, T. (2002). Runx2, a multifunctional transcription factor in skeletal development. J. Cell Biochem. *87*, 1–8.

Komori, T. (2003). Requisite roles of Runx2 and Cbfb in skeletal development. J. Bone Miner. Metab. *21*, 193–197.

Komori, T. (2008). Regulation of bone development and maintenance by Runx2. Front Biosci. *13*, 898–903.

Krek, A., Grün, D., Poy, M.N., Wolf, R., Rosenberg, L., Epstein, E.J., MacMenamin, P., da Piedade, I., Gunsalus, K.C., Stoffel, M., et al. (2005). Combinatorial microRNA target predictions. Nat. Genet. *37*, 495–500.

Krzeszinski, J.Y., Wei, W., Huynh, H., Jin, Z., Wang, X., Chang, T.C., Xie, X.J., He, L., Mangala, L.S., Lopez-Berestein, G., et al. (2014). miR-34a blocks osteoporosis and bone metastasis by inhibiting osteoclastogenesis and Tgif2. Nature *512*, 431–435.

Li, X.J., Ji, M.H., Zhong, S.L., Zha, Q.B., Xu, J.J., Zhao, J.H., and Tang, J.H. (2012). MicroRNA-34a modulates chemosensitivity of breast cancer cells to adriamycin by targeting Notch1. Arch. Med. Res. *43*, 514–521.

Li, H., Li, T., Wang, S., Wei, J., Fan, J., Li, J., Han, Q., Liao, L., Shao, C., and Zhao, R.C. (2013a). miR-17-5p and miR-106a are involved in the balance between osteogenic and adipogenic differentiation of adipose-derived mesenchymal stem cells. Stem Cell Res. *10*, 313–324.

Li, Y., Fan, L., Liu, S., Liu, W., Zhang, H., Zhou, T., Wu, D., Yang, P., Shen, L., Chen, J., et al. (2013b). The promotion of bone regeneration through positive regulation of angiogenic-osteogenic coupling using microRNA-26a. Biomaterials *34*, 5048–5058.

Lian, J.B., Stein, G.S., van Wijnen, A.J., Stein, J.L., Hassan, M.Q., Gaur, T., and Zhang, Y. (2012). MicroRNA control of bone formation and homeostasis. Nat. Rev. Endocrinol. *8*, 212–227.

Liang, X., Zeng, J., Wang, L., Fang, M., Wang, Q., Zhao, M., Xu, X., Liu, Z., Li, W., Liu, S., et al. (2013). Histone demethylase retinoblastoma binding protein 2 is overexpressed in hepatocellular carcinoma and negatively regulated by hsa-miR-212. PLoS One *8*, e69784.

Liao, Y.H., Chang, Y.H., Sung, L.Y., Li, K.C., Yeh, C.L., Yen, T.C., Hwang, S.M., Lin, K.J., and Hu, Y.C. (2014). Osteogenic differentiation of adipose-derived stem cells and calvarial defect repair using baculovirus-mediated co-expression of BMP-2 and miR-148b. Biomaterials *35*, 4901–4910.

Luzi, E., Marini, F., Sala, S.C., Tognarini, I., Galli, G., and Brandi, M.L. (2008). Osteogenic differentiation of human adipose tissue-derived stem cells is modulated by the miR-26a targeting of the SMAD1 transcription factor. J. Bone Miner. Res. *23*, 287–295.

Luzi, E., Marini, F., Tognarini, I., Galli, G., Falchetti, A., and Brandi, M.L. (2012). The regulatory network menin-microRNA 26a as a possible target for RNA-based therapy of bone diseases. Nucleic Acid Ther. *22*, 103–108.

Pang, R.T., Leung, C.O., Ye, T.M., Liu, W., Chiu, P.C., Lam, K.K., Lee, K.F., and Yeung, W.S. (2010). MicroRNA-34a suppresses invasion through downregulation of Notch1 and Jagged1 in cervical carcinoma and choriocarcinoma cells. Carcinogenesis *31*, 1037–1044.

Park, H., Park, H., Pak, H.J., Yang, D.Y., Kim, Y.H., Choi, W.J., Park, S.J., Cho, J.A., and Lee, K.W. (2015). MiR-34a inhibits differentiation of human adipose tissue-derived stem cells by regulating cell cycle and senescence induction. Differentiation *90*, 91–100.

Perisanidis, C., Perisanidis, B., Wrba, F., Brandstetter, A., El Gazzar, S., Papadogeorgakis, N., Seemann, R., Ewers, R., Kyzas, P.A., and Filipits, M. (2012). Evaluation of immunohistochemical expression of p53, p21, p27, cyclin D1, and Ki67 in oral and oropharyngeal squamous cell carcinoma. J. Oral Pathol. Med. *41*, 40–46.

Pestell, R.G. (2013). New roles of cyclin D1. Am. J. Pathol. *183*, 3–9.

Pratap, J., Galindo, M., Zaidi, S.K., Vradii, D., Bhat, B.M., Robinson, J.A., Choi, J.Y., Komori, T., Stein, J.L., Lian, J.B., et al. (2003). Cell growth regulatory role of Runx2 during proliferative expansion of preosteoblasts. Cancer Res. *63*, 5357–5362.

Qureshi, A.T., Monroe, W.T., Dasa, V., Gimble, J.M., and Hayes, D.J. (2013). miR-148b-nanoparticle conjugates for light mediated osteogenesis of human adipose stromal/stem cells. Biomaterials *34*, 7799–7810.

Sun, F., Fu, H., Liu, Q., Tie, Y., Zhu, J., Xing, R., Sun, Z., and Zheng, X. (2008). Downregulation of CCND1 and CDK6 by miR-34a induces cell cycle arrest. FEBS Lett. *582*, 1564–1568.

Sun, F., Wan, M., Xu, X., Gao, B., Zhou, Y., Sun, J., Cheng, L., Klein, O.D., Zhou, X., and Zheng, L. (2014). Crosstalk between miR-34a and Notch signaling promotes differentiation in apical papilla stem cells (SCAPs). J. Dent. Res. *93*, 589–595.

Teng, Y.C., Lee, C.F., Li, Y.S., Chen, Y.R., Hsiao, P.W., Chan, M.Y., Lin, F.M., Huang, H.D., Chen, Y.T., Jeng, Y.M., et al. (2013). Histone demethylase RBP2 promotes lung tumorigenesis and cancer metastasis. Cancer Res. *73*, 4711–4721.

Thomas, M., Lieberman, J., and Lal, A. (2010). Desperately seeking microRNA targets. Nat. Struct. Mol. Biol. *17*, 1169–1174.

Wang, S., Qu, X., and Zhao, R.C. (2011). Mesenchymal stem cells hold promise for regenerative medicine. Front Med. *5*, 372–378.

Wang, M.T., Chen, G., An, S.J., Chen, Z.H., Huang, Z.M., Xiao, P., Ben, X.S., Xie, Z., Chen, S.L., Luo, D.L., et al. (2012). Prognostic significance of cyclinD1 amplification and the co-alteration of cyclinD1/pRb/ppRb in patients with esophageal squamous cell carcinoma. Dis. Esophagus *25*, 664–670.

Wang, J., Guan, X., Guo, F., Zhou, J., Chang, A., Sun, B., Cai, Y., Ma, Z., Dai, C., Li, X., et al. (2013). miR-30e reciprocally regulates the differentiation of adipocytes and osteoblasts by directly targeting low-density lipoprotein receptor-related protein 6. Cell Death Dis. *4*, e845.

Wang, Z., Xie, Q., Yu, Z., Zhou, H., Huang, Y., Bi, X., Wang, Y., Shi, W., Sun, H., Gu, P., et al. (2015a). A regulatory loop containing miR-26a, GSK3β and C/EBPα regulates the osteogenesis of human adipose-derived mesenchymal stem cells. Sci. Rep. *5*, 15280.

Wang, Z., Zhang, D., Hu, Z., Cheng, J., Zhuo, C., Fang, X., and Xing, Y. (2015b). MicroRNA-26a-modified adipose-derived stem cells incorporated with a porous hydroxyapatite scaffold improve the repair of bone defects. Mol. Med. Rep. *12*, 3345–3350.

Wei, J., Shi, Y., Zheng, L., Zhou, B., Inose, H., Wang, J., Guo, X.E., Grosschedl, R., and Karsenty, G. (2012). MiR-34s inhibit osteoblast proliferation and differentiation in the mouse by targeting SATB2. J. Cell Biol. *197*, 509–521.

Xiao, C., Zhou, H., Liu, G., Zhang, P., Fu, Y., Gu, P., Hou, H., Tang, T., and Fan, X. (2011). Bone marrow stromal cells with a combined expression of BMP-2 and VEGF-165 enhanced bone regeneration. Biomed. Mater. *6*, 015013.

Xu, P.Z., Guo, M., and Hay, B.A. (2004). MicroRNAs and the regulation of cell death. Trends Genet. *20*, 617–624.

Yau, W.W., Rujitanaroj, P.O., Lam, L., and Chew, S.Y. (2012). Directing stem cell fate by controlled RNA interference. Biomaterials *33*, 2608–2628.

Ye, J.H., Xu, Y.J., Gao, J., Yan, S.G., Zhao, J., Tu, Q., Zhang, J., Duan, X.J., Sommer, C.A., Mostoslavsky, G., et al. (2011). Critical-size calvarial bone defects healing in a mouse model with silk scaffolds and SATB2-modified iPSCs. Biomaterials *32*, 5065–5076.

Zeng, J., Ge, Z., Wang, L., Li, Q., Wang, N., Björkholm, M., Jia, J., and Xu, D. (2010). The histone demethylase RBP2 is overexpressed in gastric cancer and its inhibition triggers senescence of cancer cells. Gastroenterology *138*, 981–992.

Zeng, Y., Qu, X., Li, H., Huang, S., Wang, S., Xu, Q., Lin, R., Han, Q., Li, J., and Zhao, R.C. (2012). MicroRNA-100 regulates osteogenic differentiation of human adipose-derived mesenchymal stem cells by targeting BMPR2. FEBS Lett. *586*, 2375–2381.

Zhang, Z.J., Zhang, H., Kang, Y., Sheng, P.Y., Ma, Y.C., Yang, Z.B., Zhang, Z.Q., Fu, M., He, A.S., and Liao, W.M. (2012). MiRNA expression profile during osteogenic differentiation of human adipose-derived stem cells. J. Cell Biochem. *113*, 888–898.

Zhang, C., Mo, R., Yin, B., Zhou, L., Liu, Y., and Fan, J. (2014a). Tumor suppressor microRNA-34a inhibits cell proliferation by targeting Notch1 in renal cell carcinoma. Oncol. Lett. *7*, 1689–1694.

Zhang, Q., Sakamoto, K., and Wagner, K.U. (2014b). D-type cyclins are important downstream effectors of cytokine signaling that regulate the proliferation of normal and neoplastic mammary epithelial cells. Mol. Cell Endocrinol. *382*, 583–592.

Zou, D., Zhang, Z., Ye, D., Tang, A., Deng, L., Han, W., Zhao, J., Wang, S., Zhang, W., Zhu, C., et al. (2011). Repair of critical-sized rat calvarial defects using genetically engineered bone marrow-derived mesenchymal stem cells overexpressing hypoxia-inducible factor-1α. Stem Cells *29*, 1380–1390.

Zuk, P.A., Zhu, M., Ashjian, P., De Ugarte, D.A., Huang, J.I., Mizuno, H., Alfonso, Z.C., Fraser, J.K., Benhaim, P., and Hedrick, M.H. (2002). Human adipose tissue is a source of multipotent stem cells. Mol. Biol. Cell *13*, 4279–4295.